Resonance-induced oscillons in a reaction-diffusion system

Vladimir K. Vanag and Irving R. Epstein
Department of Chemistry and Volen Center for Complex Systems, MS 015, Brandeis University, Waltham, Massachusetts 02454-9110, USA

(Received 18 May 2005; revised manuscript received 14 October 2005; published 3 January 2006)

A new type of oscillon that arises from interaction between subcritical Turing and wave instabilities is found in a system of reaction-diffusion equations. These oscillons can be induced resonantly by localized external periodic perturbations. This phenomenon may be useful for frequency selection and/or information processing.

DOI: 10.1103/PhysRevE.73.016201 PACS number(s): 82.40.Ck, 02.70.Uu, 68.05.Gh, 82.33.Nq

I. INTRODUCTION

Oscillons, i.e., localized, spatially stationary, temporally oscillatory structures, were first found experimentally in a vertically vibrated layer of sand [1]. They were subsequently observed in an autonomous reaction-diffusion system [2], in optical systems [3], in plasmas [4], in nonlinear Faraday fluid mechanics experiments [5], and in the Swift-Hohenberg equation [6]. The possible practical application of oscillons in memory devices or processors [2,7,8] has heightened interest in their investigation. Oscillons may originate via several scenarios, e.g., the interaction of subcritical Turing and subcritical Hopf instabilities [2] or a homoclinic bifurcation [3]. In this work we investigate a new mechanism for generating oscillons: interaction between subcritical Turing and subcritical wave instabilities, suggested in [2].

Like any oscillatory system with a characteristic frequency, an oscillon may be expected to exhibit resonance when subject to external periodic signals. If, in a spatially extended system initially in a homogeneous steady state (SS), an autonomous oscillon can arise via a subcritical bifurcation, then it should be possible to induce oscillons by a local periodic perturbation with appropriate frequency, amplitude, and spatial extent. Here we investigate such resonances in a new type of oscillon found in a model of the Belousov-Zhabotinsky (BZ) reaction dispersed in an aerosol OT [AOT=sodium bis(ethylhexyl) sulfosuccinate] water-in-oil microemulsion (BZ-AOT system). Our study is relevant to the resonant forcing of silent neurons [9] and to resonance-induced pacemakers and waves [10–12], since all these systems have subcritical (Hopf) bifurcations and involve local resonant perturbations.

In Sec. II, we discuss our model. In Secs. III and IV we perform linear stability analysis of the model and investigate numerically the behavior of a new type of oscillon. In Sec. V, the resonantly induced "steady state→oscillon" transition is studied. In Sec. VI, we examine the possible practical application of oscillons in heterogeneous media as a frequency-selection device. In Sec. VII, we explore briefly spatial resonances with two or more oscillons. We conclude in Secs. VIII and IX, noting possible links between our chemical system and biological ones.

II. MODEL

The BZ reaction [13], the oxidation of an organic substrate (usually malonic acid) by bromate in acid medium catalyzed by a catalyst, such as $Fe(phen)_3$ or $Ru(bpy)_3$, is a complex net of chemical reactions. When dispersed in water-in-oil microemulsion, it becomes even more complex [14,15]. The Field-Körös-Noyes (FKN) mechanism [16] provides a detailed description of the chemistry of the BZ reaction.

Employing such complex models to study patterns in spatially extended systems, however, is computationally challenging and tends to obscure the origins of new behaviors. Therefore one typically employs a simplified version of the full FKN model. The most popular simplified model is the three-variable Oregonator [17], which has been successful in simulating many temporal and spatial phenomena in the aqueous BZ reaction. It can be reduced to a two-variable model [18]:

$$\partial v/\partial t = [v(1-v) - hz(v-q)/(v+q)]/\varepsilon, \tag{1}$$

$$\partial z/\partial t = v - z, \tag{2}$$

where v is the dimensionless activator concentration ($[HBrO_2]$) and z is the catalyst concentration, which plays the role of inhibitor in this set of equations, while ε, q, and h are kinetic and stoichiometric parameters.

To explain the numerous patterns found experimentally in the BZ-AOT system (e.g., Turing patterns and standing waves) we have introduced two additional dimensionless variables in model (1) and (2) [19,20], u ($[Br_2]$) and radical r ($[BrO_2^{\cdot}]$), which can diffuse rapidly in the continuous oil phase and are linked by first order reactions to the inhibitor (z) and activator (v), respectively,

$$\partial v/\partial t = [v(1-v) - hz(v-q)/(v+q) - \beta v + r]/\varepsilon + D_v \Delta v, \tag{3}$$

$$\partial z/\partial t = v - z + \gamma u - \alpha z + D_z \Delta z, \tag{4}$$

$$\partial u/\partial t = (\alpha z - \gamma u)/\varepsilon_2 + D_u \Delta u, \tag{5}$$

$$\partial r/\partial t = (\beta v - r)/\varepsilon_1 + D_r \Delta r, \tag{6}$$

where the Laplacian $\Delta = \partial^2/\partial y^2$ in 1D and $\Delta = \partial^2/\partial x^2 + \partial^2/\partial y^2$ in 2D. Values of all parameters are discussed in Sec. III.

In this work, we show that the four-variable reaction-diffusion model (3)–(6) is able to describe a new type of

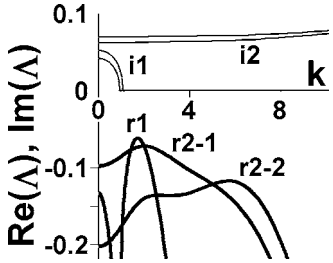

FIG. 1. Dispersion curves for system (3)–(6) for $\varepsilon_1=1.3$ and 1.5. Curves: i1, $\mathrm{Im}(\Lambda_1)/10$; i2, $\mathrm{Im}(\Lambda_2)/40$ [upper curve of two i2 (i1) curves corresponds to $\varepsilon_1=1.5(1.3)$]; r1, $\mathrm{Re}(\Lambda_1)$ (Turing peaks of curve r1 for $\varepsilon_1=1.5$ and $\varepsilon_1=1.3$ are indistinguishable); r2, $\mathrm{Re}(\Lambda_2)$. Parameters: $q=0.0025$, $h=1.2$, $\alpha=0.48$, $\gamma=0.045$, $\beta=0.65$, $\varepsilon=0.046$, $\varepsilon_1=1.5$ (r2-1) and 1.3 (r2-2), $\varepsilon_2=0.1$, $D_v=0.01$, $D_z=0.01$, $D_u=0.45$, and $D_r=0.025$.

oscillon, which may resemble the oscillon found experimentally in the BZ-AOT system [2].

In Ref. [2] we used another simplified FKN-type model to study oscillon behavior:

$$\partial v/\partial t = [v(1-v) - s(v-q) - \beta v + r]/\varepsilon + D_v \Delta v, \quad (7)$$

$$\partial z/\partial t = v - z + D_z \Delta z, \quad (8)$$

$$\partial u/\partial t = [s(q+2v) - \gamma_1 u/s]/\varepsilon_2{}' + D_u \Delta u, \quad (9)$$

$$\partial r/\partial t = (\beta v - r)/\varepsilon_1 + D_r \Delta r, \quad (10)$$

where the inhibitor s (dimensionless Br^-) is a function of z, v, and u: $s=hz/(2q+3v)+[\gamma_1 u/(2q+3v)]^{1/2}$ and h is a function of u and z: $h=h_0+u/(Kz+u)$. In Eqs. (7)–(10), the fast diffusing inhibitor u is linked both to activator v and catalyst z. Model (7)–(10) is much more complex, and therefore less preferable, than model (3)–(6).

Both models (3)–(6) and (7)–(10) have oscillon solutions. At the present stage of our understanding of patterns in the BZ-AOT system, we cannot say which model more accurately describes the experiments, though differences in the nature of the oscillon solutions found should make it possible to design experiments to distinguish between the models. There certainly exist other classes of models that also generate oscillons (as well as other patterns in the BZ-AOT system), for example, reaction-diffusion models with cross-diffusion terms, like

$$\partial v/\partial t = \text{reaction terms} + D_v \Delta v + \nabla(D_{vu} \nabla u) \quad (11)$$

where ∇ denotes gradient, and the cross-diffusion coefficient $D_{vu} \to 0$, if $v \to 0$ [21].

III. LINEAR STABILITY ANALYSIS

Typical dispersion curves for system (3)–(6) with parameters that give oscillon formation both in 1D and 2D are shown in Fig. 1. All eigenvalues Λ have negative real parts for all wave numbers k, and therefore the unperturbed system has a stable homogeneous SS. The corresponding 0D (point or well-mixed) system has only the SS solution (a stable focus) and hence cannot oscillate. Eigenvalue Λ_1 is complex at small k, while at larger k ($k>1$) it transforms into two real (negative) eigenvalues, the more positive of which (curve r1 in Fig. 1) is responsible for the subcritical Turing instability. Eigenvalue Λ_2 is complex for a broader range of k and is responsible for the wave instability.

Note that all parameters used in model (3)–(6) (see caption to Fig. 1) are physically realistic. Our values of h, ε, and q are in the range typically used in the Oregonator model. The ratio α/γ is proportional to the partition coefficient for Br_2 between the oil phase and droplet (AOT+water) pseudophase, which implies that $\alpha/\gamma \gg 1$. The coefficient β must be less than 1, since it represents the fraction of $BrO_2^{\cdot}$ radicals generated in the reaction $HBrO_2(+BrO_3^-) \to 2BrO_2^{\cdot}$ $(+2\ \text{catalyst}) \to 2HBrO_2$ that are transferred to the oil phase instead of reacting with the catalyst. We expect β to depend on the catalyst concentration, but this effect is not included in the simple model (3)–(6). Chemical considerations also imply that $\varepsilon_1 > \varepsilon$, and $\varepsilon_2 \ll 1$ [19,20].

Species v and z, which are inside water nanodroplets, diffuse with the droplets at a significantly slower speed than small molecules in the oil phase, and therefore their diffusion coefficients D_v and D_z should be approximately equal to each other and significantly smaller than the diffusion coefficients of the oil-soluble species, D_u and D_r.

The system behavior and the eigenvalues depend sensitively on the parameters. The temporal and spatial characteristics of u, ε_2, and D_u, primarily affect Λ_1, the Turing instability (curve r1 in Fig. 1), while ε_1 and D_r, the corresponding characteristics of the fast diffusing activator, r, mainly influence $\mathrm{Re}(\Lambda_2)$ and $\mathrm{Im}(\Lambda_2)$, i.e., the wave instability. It is most convenient to vary these parameters, since they leave the SS unchanged. A small increase in D_u or ε_2 leads to an increase in $\mathrm{Re}(\Lambda_1)$ and to a shift from SS to oscillons or to oscillatory Turing patterns that occupy the entire area, even while $\mathrm{Re}(\Lambda_1)$ is still negative, while increasing D_r induces changes in the opposite direction. Variations in ε_1 mainly affect the frequency of the oscillon $[\mathrm{Im}(\Lambda_2)]$. In a heterogeneous system with spatially distributed ε_1, oscillons with different frequencies can be induced.

If we vary any of the parameters individually, the range of values that yields oscillon solutions is quite narrow. If, however, we change two or more parameters simultaneously in such a way that the maxima of dispersion curves r1 and r2 in Fig. 1 remain negative and close to zero, we can find a relatively broad range of oscillon behavior. It is necessary to carry out numerical simulations for each set of parameters that potentially (from linear stability analysis) can give oscillons. Therefore elucidating in detail the regions in the parameter space where oscillon solutions occur is a time-consuming problem that we defer for future investigations. Such studies may yield a more realistic ratio between the diffusion coefficients D_u and D_r than the one employed in this work.

The oscillons originating from subcritical Hopf and Turing instabilities [2] and those found here share a common feature, seen in Fig. 1: the dispersion curves have a Turing peak (curve r1) where the relevant eigenvalue, Λ_1, is real in a range of k in which the other pertinent eigenvalue, Λ_2, is

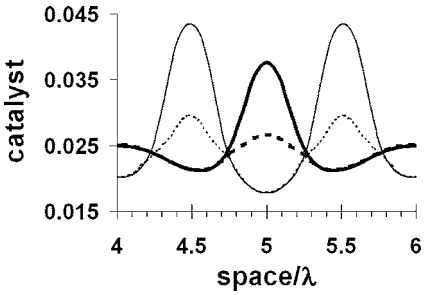

FIG. 2. Cross sections of one-hump (bold and dashed lines) and two-hump (thin and dotted lines) oscillons at maximum and minimum of z oscillation. Spatial unit $\lambda=2\pi/k_T$, $\varepsilon_1=1.5$. All other parameters as in Fig. 1.

complex (curves r2, i2). In this context we can say that the two eigenvalues interact with each other.

IV. SIMULATION OF THE OSCILLON

Our numerical simulations were carried out with the FlexPDE package [22] with periodic and with zero flux boundary conditions. FlexPDE refines the triangular finite element mesh until the estimated error in any variable is less than a specified tolerance, which we chose as 10^{-4}, at every cell of the mesh. Smaller tolerances did not change the results.

An appropriate local initial perturbation can induce oscillons like those shown in Fig. 2. We typically decrease z from its SS value z_{SS}, $z_0=z_{SS}[1-A_0'\phi(y)]$, where y is the spatial coordinate in 1D, A_0' is the amplitude of the perturbation, and $\phi(y)=0$ everywhere, except $\phi(y)=1$ for $y_1<y<y_1+L_p$ for a one-hump oscillon and in addition $\phi(y)=1$ if $y_2<y<y_2+L_p$ for a two-hump oscillon. The values y_1 and $y_2>y_1$ are arbitrary, but for coordinated behavior of two humps, the difference $y_2-y_1\equiv g$ must lie in a particular range. Note that the frequencies of one-hump and two-hump oscillons differ slightly (by about 3%). For the combination of subcritical Hopf and Turing instabilities considered in [2], different superthreshold local perturbations gave rise to both stationary and oscillatory localized peaks at the same set of model parameters. In the present case, only oscillons can be induced.

Since our oscillon is associated with a wave instability, it exhibits some properties of packet waves; specifically, it can travel at a velocity related to the group velocity, $d\,\mathrm{Im}(\Lambda_2)/dk$. For $\varepsilon_1=1.5$, $d\,\mathrm{Im}(\Lambda_2)/dk\cong 0$ at the wave number $k(\cong 2)$ where $\mathrm{Re}(\Lambda_2)$ (curve r2-1 in Fig. 1) reaches its maximum, i.e., the wave number that tends to be selected, and the pattern is stationary. For $\varepsilon_1=1.3$, in contrast, $d\,\mathrm{Im}(\Lambda_2)/dk\cong 0.04$ at $k\cong 6$ (the maximum of curve r2-2), and the oscillon can move. This movement differs in 1D and 2D. In both cases an initial single symmetric motionless oscillon is stable. To initiate movement or splitting of the oscillon, we create an asymmetry, e.g., by transiently changing D_u in a small region to the left or right of the oscillon. In experiment the asymmetry can be generated, for example, by a local thermal perturbation on one side of the oscillon. As soon as the oscillon develops some asymmetry, we return the

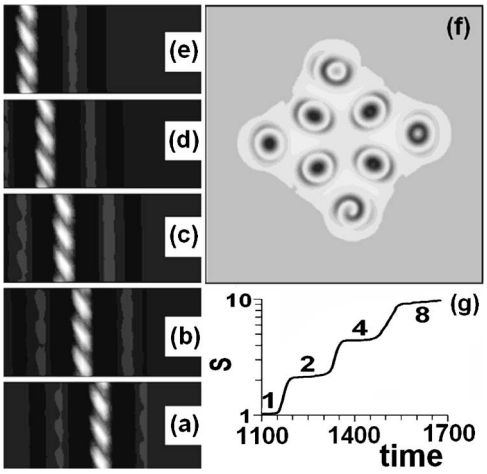

FIG. 3. (a)–(e). Moving single oscillon in 1D. Size of each frame is $4.35\lambda\times 3T_0$, where $T_0=2.588$, the period of the oscillon, $\lambda=3.6$. Frames (a)–(e) are separated by $51.12T_0$, $\varepsilon_1=1.3$, all other parameters as in Fig. 1. (f) Metastable localized structure in 2D with small localized spiral instead of oscillon near the bottom vertex. Period of the spiral is T_0. Frame size$=6\lambda\times 6\lambda$. (g) Dynamics of splitting oscillons in 2D, S is proportional to the area occupied by oscillatory patterns. Numbers at the plateaus indicate the numbers of oscillons; the last octet configuration is shown in (f).

altered parameter to its original homogeneous value. In 1D, the asymmetric oscillon starts to move with a constant velocity [see Figs. 3(a)–3(e)]. With periodic boundary conditions, the oscillon moves indefinitely without changing its shape.

The 1D moving oscillon is intermediate in character between traveling solitonlike packet waves [subcritical wave instability with positive $\mathrm{Re}(\Lambda)$ [23]] and stationary oscillons [2]. Note that solitonlike packet waves reflect from a zero-flux boundary, while moving oscillons instead produce a localized structure near the boundary, for example, two in-phase and one antiphase oscillating peaks separated by the Turing wavelength λ. When two oncoming oscillons approach one another, they give rise to a new, two-hump oscillon that can either be stationary or, after some time, begins to move.

In 2D, an initially asymmetric oscillon splits into two, and each of these new oscillons splits again perpendicular to the direction of the first splitting. The average distance between oscillons is about $\lambda=2\pi/k_T$, where k_T corresponds to the maximum of curve r1 in Fig. 1. This metastable structure of four oscillons persists for some time before producing four new oscillons [see Figs. 3(f) and 3(g)]. One of these new oscillons quickly transforms into a small localized spiral similar to the localized spirals found in a model of coupled layers [24]. This octet structure is stable for at least several tens of oscillation periods. If we suppress all oscillons except the localized spiral, that object transforms into a normal oscillon, which later undergoes a new cycle of splitting. The localized spiral arises only in asymmetric environments like that in Fig. 3(f) and is quite stable in such situations.

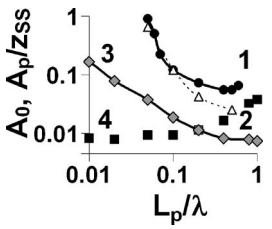

FIG. 4. Threshold amplitudes for generating oscillons. Curves 1 and 2 are A_0 in 1D and 2D, respectively; curve 3 is A_p/z_{SS} for $T_p=2.25$ in 1D; curve 4 is $5A_p \times L_p$. Parameters of system (3)–(6) as in Fig. 1, $\varepsilon_1=1.5$.

V. LOCAL PERIODIC PERTURBATION AND RESONANCES

To study resonance effects, we first determined the threshold amplitude A_0 of an initial perturbation of spatial extent L_p needed to generate a stationary one-hump oscillon (curves 1 and 2 in Fig. 4). If $L_p > \lambda$, the final pattern in 1D is the homogeneous SS, while in 2D, an initial circular perturbation with $L_p > 0.6\lambda$ leads to the generation of multiple oscillons.

We next considered time-periodic perturbations, in which Eq. (4) in 1D was augmented by a term $A_p' \sin(2\pi t/T_p)\phi(y)$, where $\phi(y)$ describes the spatial extent L_p of the perturbed zone.

$$\partial z/\partial t = v - z + \gamma u - \alpha z + A_p' \sin(2\pi t/T_p)\phi(y) + D_z \Delta z \tag{4'}$$

In our computer experiments, this external periodic local perturbation was applied until the behavior of the system became stationary, generally after $<100T_p$. Then, the perturbation was switched off, and the system relaxed either to SS or to an oscillon. The threshold values, A_p, obtained at $T_p=2.25$, close to the natural period of the oscillon, $T_0=2.305$, are presented in curve 3 of Fig. 4. A_p/z_{SS} is almost one order of magnitude smaller than A_0. For time-periodic perturbations with $L_p < 0.2\lambda$, the product $A_p \times L_p$ (see curve 4 of Fig. 4), analogous to the energy of the perturbation, is constant over nearly two orders of magnitude change in L_p. For further investigation of resonance effects, we fix $L_p/\lambda=0.2$, close to the minima of curves 1 and 3 in Fig. 4.

The time-periodic perturbation periodically increases and decreases z, while the initial perturbation considered earlier only consisted of a decrease in z below z_{SS}. We next examined how the shape of an external periodic perturbation affects the system response. With fixed L_p, we measured threshold amplitudes $A_p(f)$ as a function of frequency f for the above harmonic perturbation and for the four different shapes of square periodic perturbations shown in Fig. 5. Shapes 1 and 2 are sequences of purely activating and purely inhibitory square impulses, respectively. Shape 3 resembles the harmonic perturbation, while in shape 4, the inhibitory impulses follow immediately after the activating impulses. The ratio of impulse duration to perturbation period, τ/T_p, was set to 0.25 for all cases. Note that the behavior of $A_p(\tau/T_p)$ is similar to that of $A_p(L_p/\lambda)$ shown in Fig. 4 (curve 1), and $\tau/T_p=0.25$ lies close to the minimum of this curve.

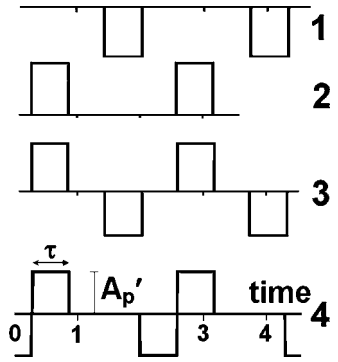

FIG. 5. Shapes of periodic square perturbations.

The results shown in Fig. 6 reveal that there are only minor differences among the curves for perturbations that contain both activating and inhibitory pulses: the harmonic and square-shaped perturbations of shapes 3 and 4 (see Fig. 5). All of these curves exhibit significant resonance effects of nearly two orders of magnitude in A_p. On the other hand, with only activating pulses (shape 2), the resonance tongues are rather shallow, while the sequence of purely inhibitory pulses (shape 1) yields almost no observable resonance. Note the relatively shallow resonance at $f:f_0=2:1$ and the absence of any resonance at $f:f_0=3:2$.

There are important differences between the resonances found in periodic forcing of existing oscillations (Arnold tongues) and the resonances in the present case of subcritical bifurcations. Figure 7(a) demonstrates oscillations for a periodic perturbation with amplitude $A_p' < A_p$ (at period $T=2.4$), while Fig. 7(b) shows the opposite case, when $A_p' > A_p$ (at $T=2.7$). When $A_p' < A_p$, the average period of oscillation is equal to the period of the external perturbations [Fig. 7(c)], while when $A_p' > A_p$ this relation holds true

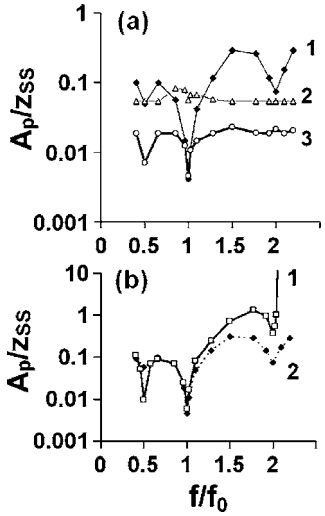

FIG. 6. Resonances $A_p(f)$. (a) 1, harmonic perturbation; 2, inhibitory pulses (shape 2 in Fig. 5); and 3, activating pulses (shape 1 in Fig. 5). (b) 1, shape 4 in Fig. 5; 2, shape 3 in Fig. 5; $f_0=1/T_0$, $T_0=2.305$. Parameters of system (3)–(6) as in Fig. 1, $\varepsilon_1=1.5$.

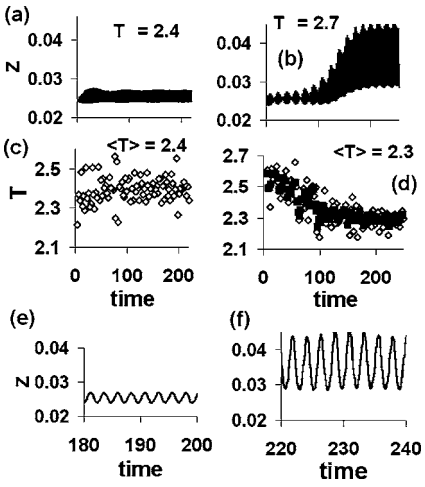

FIG. 7. Oscillations in system (3)–(6) under local periodic perturbation (shape 4 in Fig. 5) with period T at (a) $A_p' < A_p$ and (b) at $A_p' > A_p$. All system parameters as in Fig. 1, $\varepsilon_1 = 1.5$. (c) and (d) show dependences (open rhombs) of time intervals between neighboring maxima of oscillations shown in (a) and (b), respectively, on time. Averaged intervals $\langle T \rangle$ are taken for those times when the shape of oscillations does not change with time [for (d), *time* > 180]. Filled squares in (d) are 3-point running averages of time intervals between neighboring maxima. Panels (e) and (f) are enlarged segments of (a) and (b), respectively.

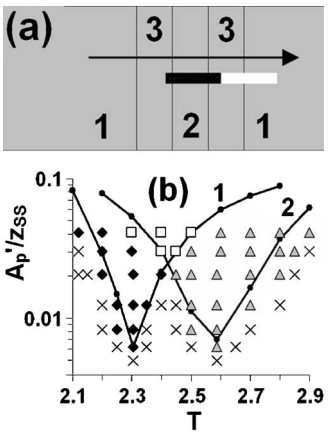

FIG. 8. Resonance induced oscillons in a heterogeneous medium. (a) In zone 1, $\varepsilon_1 = 1.5$, $D_u = 0.445$, $D_r = 0.025$; in zone 2, $\varepsilon_1 = 1.3$, $D_u = 0.45$, $D_r = 0.025$; in zone 3, $\varepsilon = 0.05$, $\varepsilon_1 = 1.6$, $D_u = 0.1$, $D_r = 0.015$. System size $= 9\lambda \times 4\lambda$, $\lambda = 3.6$; perturbing impulse runs in a band of size $6.5\lambda \times \lambda/4$. All other parameters as in Fig. 1. (b) Phase diagram in the $T_p - A_p'/z_{SS}$ plane for computer experiments described in (a), $T_p = L/v$; ×, no oscillons; ♦, oscillons in zone 1 only; ▲, oscillon in zone 2 only; and □, oscillons in both zones 1 and 2. Curves (1) and (2) are threshold values A_p/z_{SS} obtained in 1D for system (3)–(6) with $\varepsilon_1 =$ (curve 1) 1.5, (curve 2) 1.3.

only initially. As the amplitude of oscillation increases, the period tends to the natural period T_0 of the unperturbed oscillon [Fig. 7(d)]. Figures 7(e) and 7(f) present enlargements of segments from Figs. 7(a) and 7(b), respectively. Since the system actually possesses two frequencies, f_0 ($= 1/T_0$ with large amplitude) and f ($= 1/T$ with small amplitude), beats can be seen in Fig. 7(b). In the case of frequency locking in Arnold tongues, the system oscillates only at the frequency of the external perturbation (1:1 resonance) or its subharmonics.

VI. FREQUENCY SELECTION IN A HETEROGENEOUS MEDIUM

The deep resonance at $f : f_0 = 1 : 1$ can be used for resonant induction of oscillons in a heterogeneous medium. To demonstrate this possibility, we consider a system consisting of five zones [Fig. 8(a)]. In the two zones labeled "1," $\varepsilon_1 = 1.5$; the central zone "2" has $\varepsilon_1 = 1.3$. In a 1D homogeneous system, zones 1 and 2 would exhibit the resonances shown in Fig. 8(b) by curves 1 and 2, respectively. The two "inert" zones "3" support only SS. We attempt to initiate oscillons in this system starting from the homogeneous SS. We construct an impulse [narrow black and white horizontal bars in Fig. 8(a), corresponding to activating and inhibitory perturbations, respectively] that moves with velocity v and frequency v/L from left to right along a segment of length L equal to the length of the arrow in Fig. 8(a) and crosses all five zones (the outer portion of each zone 1 is left unperturbed). The length R_p of the black and white zones of the impulse is chosen so that $R_p/L = \tau/T_p = 0.25$, where τ and T_p characterize perturbation 4 in Fig. 5. Therefore each point on the perturbed segment experiences the shape 4 perturbation in Fig. 5. This system is analogous to a chain of excitable cells perturbed at a constant frequency through a long neuron.

The behavior of the system is summarized in Fig. 8(b). Two examples of resulting oscillons obtained for $A_p'/z_{SS} = 0.02$ at $L/v = T_{01}$ (=2.305, the natural period of oscillons in zone 1) and $L/v = T_{02}$ (=2.588, the natural period of oscillons in zone 2) are presented in Figs. 9(a) and 9(b), respectively. Since the width of each zone is equal to λ, at most one oscillon can form per zone. As seen in Fig. 8(b), if the parameters A_p' and v lie near the tip of tongue 1 (2), then

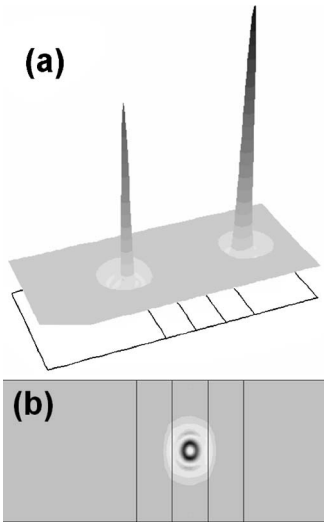

FIG. 9. (a) Contour map of oscillons (vertical axis is z) that emerge in zones 1 (see Fig. 8) when the period of the impulse is 2.305. (b) Oscillon in zone 2 (see Fig. 8) for a perturbing impulse of period 2.588.

oscillons emerge only in zone 1 (2). The small deviation from the behavior predicted by curves 1 and 2 arise (a) because the curves are calculated in 1D and (b) from perturbations caused by the boundaries with zone 3 in our heterogeneous 2D medium. At larger A_p', where tongues 1 and 2 overlap, oscillons can emerge in both zones 1 and 2.

The ability of such a system to discriminate between impulses of different frequencies offers the possibility of constructing devices for filtering and spatially sorting signals according to their frequencies. We analyzed mixed perturbations of the form $[A_{p1}' \sin(2\pi t/T_{p1}) + A_{p2}' \sin(2\pi t/T_{p2})]\phi(y)$ in 1D and analogous mixed impulses with different velocities v in 2D in geometries analogous to Fig. 8(a). In both cases, a mixed impulse induces an oscillon in a zone if and only if A_{pi}' exceeds $A_p(T_{pi})$, the critical amplitude [Fig. 8(b)] at T_{pi}, for at least one of the components of the impulse.

Our preliminary experiments on periodic and constant illumination of the photosensitive $Ru(bpy)_3$–catalyzed BZ-AOT system reveal that stationary (Turing) patterns can be transformed to oscillatory (global or localized) patterns above a threshold intensity of light. The frequency of the oscillatory patterns may depend on the light intensity. By illuminating the BZ-AOT system through spatially structured masks, a desired spatial heterogeneity can be imprinted [25–28]. The moving impulse can be created by a laser beam, which can induce and suppress oscillations. The combination of constant illumination through a mask with a moving light beam can create arrangements like that shown in Fig. 8(a), where the system parameters take on different values in chosen regions.

Thus, as our example of frequency selection shows, oscillons can be used not only for memory devices but also for signal processing.

VII. SPATIAL RESONANCE IN A HOMOGENEOUS MEDIUM

In contrast to homogeneous systems with only a subcritical Hopf bifurcation [12], our homogeneous system with subcritical wave and Turing instabilities can respond locally and resonantly to local periodic perturbations. As noted above, two-hump oscillons have a slightly smaller frequency than one-hump oscillons, which allows the possibility of spatial resonance when we introduce two local periodic impulses separated in space by a gap, $g=y_2-y_1$. The dependence of the critical amplitude A_p on g for two identical impulses with period $T=2.2$ is shown in Fig. 10. This dependence has a minimum, $A_{p\text{-min}}$, at $g/\lambda \cong 1$. As g is increased, A_p plateaus at $A_{p\text{-pl}}$ ($=A_p$ for a single impulse, $A_{p\text{-pl}}/A_{p\text{-min}} \cong 1.5$ and 1.8 for $T=2.2$ and 2.1, respectively) at $g>(3-4)\lambda$; for smaller gaps A_p rises to $4A_{p\text{-min}}$ at $g\cong 0.5\lambda$. At $g<0.5\lambda$, two external impulses generate a single oscillon (i.e., the two perturbations merge). Thus, if we take two impulses with amplitude A_p' just slightly larger then $A_{p\text{-min}}$ [e.g., $A_p'=(1.1-1.3)A_{p\text{-min}}$] and separated by $g=\lambda$, we obtain a two-hump oscillon. Impulses with the same amplitude A_p' but separated by $g=(2-3)\lambda$ [or by $g=(0.5-0.8)\lambda$] decay to SS, since for this gap range, $A_p'<A_p$. Figure 11 illustrates this behavior, which is a form of spatial resonance, since the emergence of oscillons depends only on the distance between the two impulses. Similar behavior was observed in the spatial resonance of Turing patterns [26].

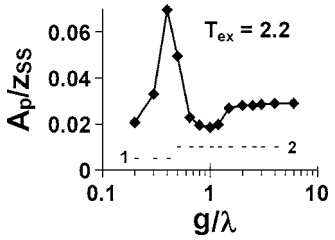

FIG. 10. Dependence (rhombs) of the threshold amplitude A_p (shown as A_p/z_{SS}) on the gap g between two synchronous local perturbations with period $T_{ex}=2.2$ (shape 4 in Fig. 5) in 1D. Numbers 1 and 2 near the horizontal dashed lines indicate how many oscillons emerge in the system after perturbation. System (3)–(6) has parameters as in Fig. 1 with $\varepsilon_1=1.5$.

VIII. CONCLUSION

We have shown that localized oscillatory solutions of reaction-diffusion equations, like Eqs. (3)–(6), can arise from interaction between subcritical wave and Turing instabilities. Localized periodic perturbation of a homogeneous medium that supports oscillon solutions can resonantly induce oscillons (1:1, 1:2, and 2:1 resonances). The ability to generate oscillons by local perturbations opens the possibility of applications such as memory devices or spatial filtering. Preliminary experiments in our laboratory on the photosensitive BZ-AOT system demonstrate that when the system is in the region of subcritical Turing instability and simultaneously near a region of oscillatory instability (Hopf or wave), it can preserve the image of a complex mask, supporting the numerical calculations presented in this work.

IX. OUTLOOK

Other localized oscillatory patterns in systems with subcritical bifurcations should exhibit analogous resonances. One possible instance involves the transmission of informa-

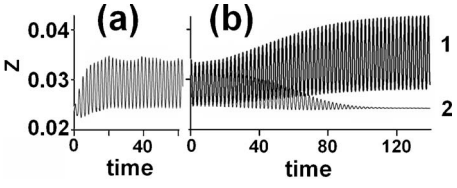

FIG. 11. Spatial resonance in a system (3)–(6) with parameters as in Fig. 1 except $\varepsilon_1=1.5$ and $D_u=0.445$. Two external synchronous local perturbations with amplitude $A_p'=0.0013$ and period $T=2.1$ (shape 4 in Fig. 5) are separated in space by $g=$(curve 1) λ and (curve 2) 2λ. Oscillations in (a) and (b) are shown at a single spatial point at the center of one external perturbation; the system is shown (a) during perturbations (perturbation starts at $t=0$) and (b) after perturbation (perturbation stops at $t=0$). Curves 1 and 2 in (a) are identical.

tion from a neuron plasma membrane to the cell nucleus [29,30]. An appropriate frequency of action potentials (in the form of postsynaptic bursting signals, the analog of our external perturbation) may induce intracellular Ca^{2+} waves or oscillations (analog of our oscillons) that, in turn, may activate genes in a nucleus. In addition to potential applications of oscillons for memory [2,7,8], the examples considered above of spatial resonances and frequency-selection with the aid of oscillon solutions in reaction-diffusion systems suggest that living systems may make use of similar mechanisms to carry out information storage and processing.

ACKNOWLEDGMENTS

This work was supported by Grant No. CHE-0306262 from the Chemistry Division of the National Science Foundation and by the donors of the American Chemical Society Petroleum Research Fund.

[1] P. B. Umbanhowar, F. Melo, and H. L. Swinney, Nature (London) **382**, 793 (1996).
[2] V. K. Vanag and I. R. Epstein, Phys. Rev. Lett. **92**, 128301 (2004).
[3] D. Gomila, M. A. Matias, and P. Colet, Phys. Rev. Lett. **94**, 063905 (2005).
[4] L. Stenflo and M. Y. Yu, Phys. Plasmas **10**, 912 (2003).
[5] I. V. Barashenkov, N. V. Alexeeva, and E. V. Zemlyanaya, Phys. Rev. Lett. **89**, 104101 (2002).
[6] I. S. Aranson and L. S. Tsimring, Physica A **249**, 103 (1998).
[7] S. Barland *et al.*, Nature (London) **419**, 699 (2002).
[8] P. Coullet, C. Riera, and C. Tresser, Chaos **14**, 193 (2004).
[9] P. Parmananda, C. H. Mena, and G. Baier, Phys. Rev. E **66**, 047202 (2002).
[10] G. Baier, S. Sahle, J. P. Chen, and A. A. Hoff, J. Chem. Phys. **110**, 3251 (1999).
[11] G. Baier and M. Muller, Phys. Lett. A **330**, 350 (2004).
[12] P. Parmananda, H. Mahara, T. Amemiya, and T. Yamaguchi, Phys. Rev. Lett. **87**, 238302 (2001).
[13] A. M. Zhabotinsky, Proc. Acad. Sci. USSR **157**, 392 (1964).
[14] V. K. Vanag and D. V. Boulanov, J. Phys. Chem. **98**, 1449 (1994).
[15] V. K. Vanag and I. Hanazaki, J. Phys. Chem. **100**, 10609 (1996).
[16] R. J. Field, E. Körös, and R. M. Noyes, J. Am. Chem. Soc. **94**, 8649 (1972).
[17] R. J. Field and R. M. Noyes, J. Chem. Phys. **60**, 1877 (1974).
[18] J. P. Keener and J. J. Tyson, Physica D **21**, 307 (1986).
[19] V. K. Vanag and I. R. Epstein, Phys. Rev. Lett. **87**, 228301 (2001).
[20] V. K. Vanag and I. R. Epstein, Phys. Rev. Lett. **88**, 088303 (2002).
[21] D. G. Leaist, Phys. Chem. Chem. Phys. **4**, 4732 (2002).
[22] FlexPDE, http://www.pdesolutions.com (2001).
[23] V. K. Vanag and I. R. Epstein, J. Chem. Phys. **121**, 890 (2004).
[24] L. Yang and I. R. Epstein, Phys. Rev. Lett. **90**, 178303 (2003).
[25] I. Berenstein, M. Dolnik, A. M. Zhabotinsky, and I. R. Epstein, J. Phys. Chem. A **107**, 4428 (2003).
[26] M. Dolnik, I. Berenstein, A. M. Zhabotinsky, and I. R. Epstein, Phys. Rev. Lett. **87**, 238301 (2001).
[27] T. Sakurai, E. Mihaliuk, F. Chirila, and K. Showalter, Science **296**, 2009 (2002).
[28] V. K. Vanag *et al.*, Nature (London) **406**, 389 (2000).
[29] M. J. Berridge, Neuron **21**, 13 (1998).
[30] R. D. Fields and P. G. Nelson, J. Neurobiol. **25**, 281 (1994).